Structure of a Murine Leukemia Virus Receptor-Binding Glycoprotein at 2.0 Angstrom Resolution

Nonhandled animals were completely undisturbed until day 12 of life at which time normal cage maintenance was initiated. The behavior of each dam was observed [M. M. Myers, S. A. Brunelli, H. N. Shair, J. M. Squire, M. A. Hofer, *Dev. Psychobiol.* **22,** 55 (1989)] for eight 60-min observation periods daily for the first 10 days after birth with six periods during the light phase and two periods during the dark phase of the L:D cycle. The distribution of the observations was based on the finding that nursing in rats occurs more frequently during the light phase of the cycle. Handling occurred each day at 1100, and an observation was scheduled at 1130 to correspond to the reunion of the mothers and pups. Within each observation period the behavior of each mother was scored every 4 min (15 observations per period × 8 periods per day = 120 observations per mother per day) for mother off pups, mother licking and grooming any pup, or mother nursing pups in either an arched-back posture, a "blanket" posture in which the mother lies over the pups, or a passive posture in which the mother lies either on her back or side while the pups nurse. Behavioral categories are not mutually exclusive.

17. D. Liu *et al.*, data not shown.
18. Nine Long-Evans female rats were mated in our animal facility and housed and observed as described (*16*). The animals underwent routine cage maintenance beginning on day 12 but were otherwise not manipulated. At the time of weaning on day 22 of life, the male offspring were housed in same-sex, same-litter groups. Testing of offspring occurred no earlier than 100 days of age.
19. We then rank-ordered the dams on licking and grooming, identifying those mothers whose scores fell above the mean, and as a group these dams were classified as high LG-ABN. The remaining dams were classified as low LG-ABN. The offspring were tested beginning at 100 days of age.
20. For restraint stress (20 min) testing (*6*), two animals from each of the nine litters were randomly selected for testing. Blood samples were collected from indwelling right jugular vein catheters (*6*), implanted 4 days before restraint stress testing, and replaced with an equal volume of normal saline (0.9%) via the same route. We have found that by 72 hours after surgery, basal ACTH and corticosterone levels have returned to normal (*6*). Plasma corticosterone was measured by radioimmunoassay [L. C. Krey *et al.*, *Endocrinology* **96,** 1088 (1975)]. Plasma (25 μl) ACTH was measured by radioimmunoassay as described [C.-D. Walker, S. F. Akana, C. S. Cascio, M. F. Dallman, *ibid.* **127**, 832 (1990); V. Viau and M. J. Meaney, *ibid.* **129**, 2503 (1991)]. All samples were run within a single assay. In our lab the intra- and interassay coefficients of variation are 7 and 10%, respectively, for corticosterone and 8 and 11% for ACTH. The data were analyzed by two-way analyses of variance (ANOVA) with one between (group) and one within (sample) measure. Post hoc analysis was performed by Tukey test.
21. We used a delayed negative-feedback paradigm [M. Keller-Wood and M. F. Dallman, *Endocr. Rev.* **5**, 1 (1984)] in which animals are steroid-treated 2 to 4 hours before acute stress. The animals used in this study were the same animals prepared with jugular catheters for acute restraint testing. The animals were tested 4 days after restraint stress, and all but one of the catheters remained patent during this interval. The critical measure here is the ability of the steroid to inhibit subsequent HPA responses to stress. Animals were injected subcutaneously with either vehicle alone or a low to moderate dose of corticosterone (1 mg/kg in ethanol:saline/1:9) on the basis of earlier studies (*6*) showing that this dose discriminates feedback sensitivity in handled versus nonhandled rats. Restraint stress was done as described above and plasma samples were obtained from jugular catheters immediately before and at the end of the 20-min period of restraint, a time point that corresponds to the peak plasma ACTH level (*6*). The percentage suppression of plasma ACTH responses to stress for the high– versus low–LG-ABN groups was derived by comparing Δ(peak stress level − basal level) for each of the corticosterone-treated animals in both groups

with that of the mean for the respective control groups (vehicle-treated high– or low–LG-ABN animals). Percentage suppression scores were used to accommodate for the groups differences in plasma ACTH responses to acute stress. The results were examined statistically by Mann-Whitney U test on the basis of percentage scores.

22. CRH mRNA in situ hybridization was done with a 48–base pair (bp) oligonucleotide sequence (CAGTTTCCTGTTGCTGTGAGCTTGCTGAGCTA-ACTGCTCTGCCCTGGC) (Perkin-Elmer,Warrington, UK) and a modified version of the procedure previously described [N. Shanks, S. Larocque, M. J. Meaney, *J. Neurosci.* **15**, 376 (1995)] with brain sections obtained from animals rapidly killed under resting-state conditions. After hybridization, sections were apposed to Hyperfilm (Amersham) for 21 days along with sections of ^{35}S-labeled standards prepared with known amounts of radiolabeled ^{35}S in a brain paste. The hybridization signal within the parvocellular subregion of the PVNh was quantified by densitometry with an MCID image analysis system (Imaging Research, St. Catherine's, Ontario, Canada). The data are presented as arbitrary absorbance units after correction for background. These data were analyzed by *t* test for unpaired groups.

23. P. M. Plotsky, *J. Neuroendocrinol.* **3**, 1 (1991); W. H. Whitnall, *Prog. Neurobiol.* **40**, 573 (1993).

24. GR in situ hybridization was done as described [(*9*); J. R. Seckl, K. L. Dickson, G. Fink, *J. Neuroendocrinol.* **2**, 911 (1990)] with [^{35}S]UTP-labeled cRNA antisense probes transcribed with T7 RNA polymerase from a 674-bp Pst I–Eco RI fragment of the rat GR cDNA linearized with Ava I. After hybridization, sections were dehydrated, dried, and dipped in photographic emulsion (NTB-2, Kodak), and then stored at 4°C for 21 days before development and counterstaining with Cresyl Violet. The hybridization signal within dorsal hippocampal subregions was quantified by grain counting within high-power microscopic fields under brightfield illumination. Grain counting

was performed by an individual unaware of the group from which the slide was derived. For each cell field, grains over ~40 to 50 individual neurons per section were counted, on three sections per animal (*9*). After subtraction of background (grains over neuropil), mean values were derived for each hippocampal cell field for each animal. Background ranged between 10 and 15% of values found over hippocampal cells. Grain counts are presented as a function of cell area to account for possible morphological differences [J. T. McCabe, R. A. Desharnais, D. W. Pfaff, *Methods Enzymol.* **168**, 822 (1989)]. These data were analyzed by two-way ANOVA with one between measures (group) and one repeated measure (hippocampal sub-field) by Tukey post hoc test.

25. R. M. Sapolsky, L. C. Krey, B. S. McEwen, *Proc. Natl. Acad. Sci. U.S.A.* **81**, 6174 (1984); R. M. Sapolsky, M. P. Armanini, D. R. Packan, S. W. Sutton, P. M. Plotsky, *Neuroendocrinology* **51**, 328 (1990); J. L. W. Yau, T. Olsson, R. G. M. Morris, M. J. Meaney, J. R. Seckl, *Neuroscience* **66**, 571 (1995).

26. C. M. Kuhn, G. E. Evoniuk, S. M. Schanberg, *Science* **204,** 1034 (1978); S. R. Butler, M. R. Suskind, S. M. Schanberg, *ibid.* **199,** 445 (1978); S. Levine, *Ann. N.Y. Acad. Sci.* **746,** 260 (1994); C. L. Moore, *Dev. Psychobiol.* **17**, 347 (1984); M. M. Myers, H. N. Shair, M. A. Hofer, *Experientia* **48,** 322 (1992); S. M. Schanberg and T. M. Field, *Child Dev.* **58,** 1431 (1987).

27. M. A. Hofer, in L. A. Rosenblum and H. Moltz, Eds., *Symbiosis in Parent-Offspring Interactions* (Plenum, New York, 1983), pp. 61–75.

28. We thank R. Meisfeld (Univ. of Arizona) for rat GR cDNA and H. Anisman and M. Hofer for comments on an earlier version of this manuscript. Supported by grants from the Medical Research Council of Canada (MRCC) (M.J.M.) and the National Institute of Mental Health (P.M.P. and M.J.M.). M.J.M. is the recipient of an MRCC Scientist award. D.L. is a graduate fellow of the MRCC.

2 May 1997; accepted 31 July 1997

Structure of a Murine Leukemia Virus Receptor-Binding Glycoprotein at 2.0 Angstrom Resolution

Deborah Fass, Robert A. Davey, Christian A. Hamson, Peter S. Kim,* James M. Cunningham,* James M. Berger

An essential step in retrovirus infection is the binding of the virus to its receptor on a target cell. The structure of the receptor-binding domain of the envelope glycoprotein from Friend murine leukemia virus was determined to 2.0 angstrom resolution by x-ray crystallography. The core of the domain is an antiparallel β sandwich, with two interstrand loops forming a helical subdomain atop the sandwich. The residues in the helical region, but not in the β sandwich, are highly variable among mammalian C-type retroviruses with distinct tropisms, indicating that the helical subdomain determines the receptor specificity of the virus.

Retroviruses are simultaneously a profound human medical problem and a potential medical solution. They can be pathogenic, causing immunodeficiency, leukemia, and neurological disease, but they are also actively studied for their proposed utility as gene therapy vectors. Essential to both roles is the targeting of the virus to the host cell through interactions between viral envelope proteins and cell surface proteins.

Retrovirus envelope glycoproteins (*1*) are

synthesized as single chain precursors that are subsequently cleaved into two subunits, the surface (SU) and the transmembrane (TM) (Fig. 1). The SU glycoprotein binds the receptor. The TM subunit contains the hydrophobic fusion peptide and transmembrane segments and is likely to participate directly in the fusion of the viral and cellular membranes after receptor binding.

Efforts to understand the structural basis of retroviral binding and entry and to devel-

op retrovirus-based gene therapy vectors (*2*) with engineered tropisms have been hindered by the lack of high-resolution models

D. Fass and P. S. Kim, Howard Hughes Medical Institute, Whitehead Institute for Biomedical Research, Department of Biology, Massachusetts Institute of Technology, Cambridge, MA 02142, USA.
R. A. Davey, C. A. Hamson, J. M. Cunningham, Howard Hughes Medical Institute, Division of Hematology, Department of Medicine, Brigham and Women's Hospital, Harvard Medical School, Room 30, Thorn Building, 20 Shattuck Street, Boston, MA 02115, USA.
J. M. Berger, Whitehead Institute for Biomedical Research, Cambridge, MA 02142, USA.

*To whom correspondence should be addressed.

for the receptor-binding regions of retrovirus envelope glycoproteins. To address this problem, we initiated structural studies on the envelope glycoprotein of the mammalian C-type retrovirus, Friend murine leukemia virus (Fr-MLV). The cellular receptor for Fr-MLV and other ecotropic MLVs (*3*) is the 14–transmembrane-pass cationic amino acid transporter MCAT-1 (*4*). The receptor-binding function of Fr-MLV has been localized to the NH_2-terminal region of the SU glycoprotein (*5*, *6*), which has been defined as a domain by proteolysis (*7*); thus, we refer to this region as the Friend receptor-binding

domain (Fr-RBD) (Fig. 1). Here, we present the x-ray crystal structure (*8*) of Fr-RBD at 2.0 Å resolution (Table 1).

The Fr-RBD is a roughly L-shaped molecule consisting of a lopsided antiparallel β sandwich and a helical subdomain formed from two extended loops of the sandwich (Fig. 2, A and B). Six strands (strands 1, 2, 4, 5, 8, and 9) form the large sheet of the Fr-RBD sandwich, whereas three strands (strands 3, 6, and 7) make up the second face (*9*). The large sheet is curved to form nearly half a barrel, and the small sheet packs against the half-barrel at an angle of about 40°. The first loop of the helical subdomain (between strands 3 and 4) contains two α helices (helices A and D). Also within this loop is an extended coil from Leu^{50} to Thr^{100} that passes almost 360° around the end of the helical lobe. The second loop (between strands 6 and 7) contains an α helix (helix G) that packs in an antiparallel orientation against helix D. Fr-RBD contains six disulfide bonds, four of which Linder and co-workers had previously identified biochemically and two of which they had predicted correctly by computer modeling (*10*). Although the overall tertiary structure of Fr-RBD is unique, a comparison of the Cα coordinates of Fr-RBD against all known folds (*11*) reveals modest similarity between the Fr-RBD β sandwich and proteins with immunoglobulin (Ig) folds (*12*) (Fig. 3).

Amino acid sequence alignments of receptor-binding domains from C-type MLVs that use distinct receptors have highlighted regions that vary with tropism

Fig. 1. Domain organization of the Fr-MLV envelope glycoprotein and sequence of Fr-RBD. (**A**) The Fr-MLV envelope glycoprotein is synthesized as a single polypeptide chain, shown schematically (SS, signal sequence; FP, fusion peptide region; TM, transmembrane segment). Maturation involves removal of the signal sequence, cleavage to generate distinct SU and TM subunits, and removal of a short peptide at the COOH-terminus. Cleavage sites are indicated by dotted lines. The crystallized Fr-RBD region is shaded. Amino acid residues at the junctions of each indicated segment are numbered. (**B**) Secondary structural elements are indicated above the amino acid sequence of Fr-RBD. β strands are numbered and shown as black bars, with strand 3 dotted because it does not classify as a true strand (*9*). α helices are lettered and shown as gray bars and 3_{10} helices are dotted in gray. N-linked glycosylation sites are underlined. Regions conserved among MLVs are boxed in gray, whereas regions with lengths and sequences that vary with the tropism of the virus are boxed in blue and labeled VRA, VRB, and VRC (*13*). N, NH_2-terminus; C, COOH-terminus.
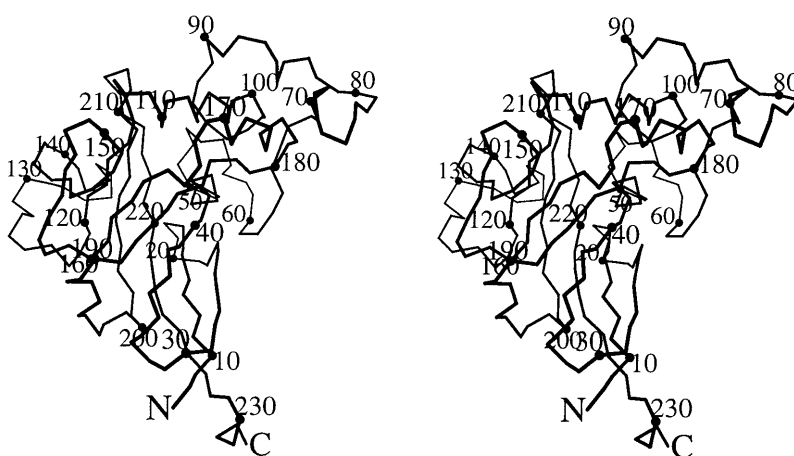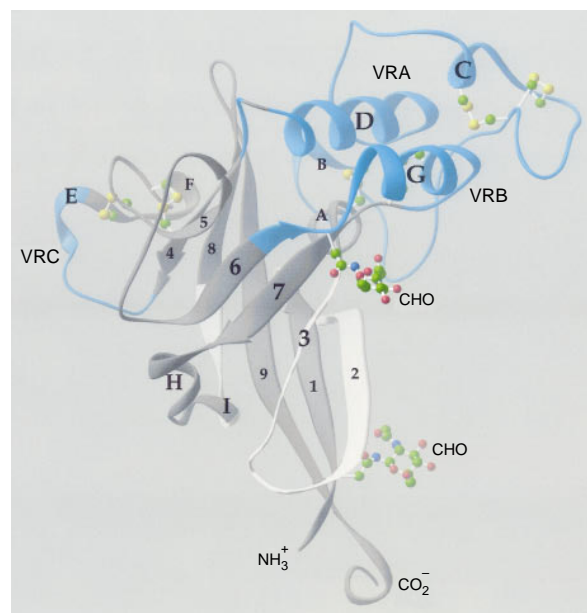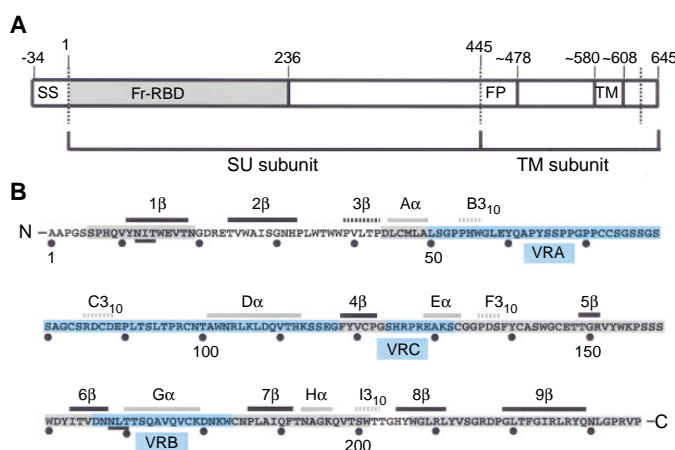

Fig. 2. Structure of Fr-RBD. (**Left**) A ribbon representation is shown with disulfide bonds and carbohydrates indicated as balls and sticks. Strands are numbered and helices are lettered to correspond to Fig. 1. Variable regions are indicated (*13*). VRA includes the extended coil in the helical subdomain (residues 50 to 100) and helix D, and VRB corresponds to helix G. VRC is located in the loop between strands 4 and 5 and is separated from VRA and VRB in the Fr-RBD structure by conserved elements such as strands 4, 5, 8, and 9 (*16*). The figure was generated with Ribbons (*36*). (**Right**) A stereo diagram of Fr-RBD is numbered every 10 residues. The figure was generated with Molscript (*37*).

(Fig. 1). These variable regions, called VRA, VRB, and VRC (*13*), are mapped onto the Fr-RBD structure in Fig. 2A. The sequence throughout most of the β sandwich is conserved, whereas the sequence corresponding to the helical lobe is highly divergent. VRA, VRB, and, to a lesser extent, VRC vary in length as well as in sequence between MLVs with different tropisms. For example, VRA in amphotropic MLVs is considerably shorter than VRA of ecotropic MLVs (61 residues and one putative disulfide bond compared with 98 residues and three disulfides bonds), whereas amphotropic VRB is longer by 19 residues, including two additional cysteines. The pattern of sequence conservation in the receptor-binding domains of MLVs, when viewed in light of the Fr-RBD structure, indicates that the Ig-like core is used as a scaffold for displaying the receptor-binding regions of the envelope glycoprotein.

Chimeric envelope proteins have been constructed by others in attempts to localize the receptor-choice determinants in MLV SU glycoproteins. Although functional chimeras can be constructed readily between various nonecotropic viruses (*14*), it has not been possible to construct functional chimeras containing both ecotropic and nonecotropic variable regions (*15*). Upon examination of the Fr-RBD structure, this observation is not surprising. VRA and VRB are intimately associated with one another in the helical lobe, and a significant alteration of the length and sequence of either VRA or VRB alone would not easily be accommodated by the rest of the structure (*16*).

Despite the absence of useful chimeras, mutagenesis experiments have identified amino acids in the VRA region of the Moloney murine leukemia virus (Mo-MLV) SU that, when altered, inhibit MCAT-1 binding without affecting envelope processing and assembly into virions (*17*). Substitution of Lys for Asp[84] in Mo-MLV SU (corresponding to Asp[86] in the closely related Fr-MLV) blocks binding and infec-tion. When residues Arg[83], Glu[86], and Glu[87] in Mo-MLV (homologous to Arg[85], Asp[88], and Glu[89] in Fr-MLV) are changed individually to Glu, Lys, and Lys, respectively, binding is abrogated, although virus titer is not significantly affected (*18*). The binding surface defined by the positions of these mutants is a textured landscape that includes a hydrophobic pocket and a charged ridge (Fig. 4).

The Fr-RBD structure demonstrates that, in the SU glycoproteins of MLVs, the polypeptide chain is partitioned structurally into a conserved Ig-like antiparallel β-sheet framework and a variable subdomain. The Fr-RBD architecture will therefore facilitate the development of viruses with novel receptor specificities for the purpose of gene therapy. Current approaches have included tethering large binding domains such as single-chain antibodies to the NH_2-terminus of the envelope protein (*19*) or substituting erythropoietin in place of SU sequences (*20*). The resultant recombinant viruses have very low transduction efficiencies and in some cases (*20*) require the wild-type glycoprotein to be co-incorporated into virions. With the use of the Fr-RBD structure as a model, modifications can now be directed to the receptor-binding lobe alone, with a detailed understanding of how the components of this subdomain interact with one another and with the core of the protein. The feasibility of replacing the variable subdomain sequences to generate

Table 1. Multiple isomorphous replacement and refinement statistics. Diffraction data were collected by means of a rotating anode source (Rigaku RU200) with an RAXIS IIc detector. All data were collected at −180°C with a Molecular Structure Corporation cryogenic crystal cooler (X stream). Crystals were mounted in a 20-μm rayon fiber loop and flash-frozen in the gaseous nitrogen stream. Reflections [average $I/\sigma(I)$ of 10.6] were indexed and integrated with the program DENZO (*28*) and were scaled with SCALEPACK (*28*). Subsequent data manipulations were carried out with the CCP4 package (*29*). We accomplished heavy atom derivatization by harvesting crystals into reservoir solution, adding solid heavy atom to 1 mM, and soaking overnight. Heavy atom sites were located for each derivative by Patterson methods. Heavy atom refinement and phasing (overall figure of merit 0.599) were carried out with MLPHARE (*30*), and the sites for each derivative were verified by calculation of difference Fourier maps with the use of phases from all other derivatives. Density modification was performed on the MIR map with the program DM (*31*). The 3 Å, density-modified map was displayed with the program O (*32*) for tracing of the polypeptide chain. The model was refined against data to 2.0 Å with the program X-PLOR (*33*). Cycles of positional refinement, temperature factor refinement, and rebuilding were continued until the free R factor (*34*) fell below 35%, at which point ordered waters were added and a bulk solvent correction was applied. The quality of the structure was verified by Procheck (*29*), with no residues falling in disallowed regions of Ramachandran space, and by 1D-3D (*35*), which gave a score consistent with all side chains being located in acceptable environments.

Parameter	Native	HgCl$_2$	Pt(II)(2,2′:6′,2″-terpyridine)Cl	Phenyl-HgAc	AgNO$_3$	PtCN$_4$
Resolution (Å)	2.0	3.0	3.0	4.0	3.0	3.0
R_{sym}* (%)	6.7	13.5	10.7	7.9	7.9	15.9
Completeness (%)	97.2	99.6	99.2	84.4	98.6	80.2
R_{iso}† (%)		22.0	20.4	20.0	15.8	19.7
Number of sites		4	1	4	4	2
Phasing power‡		1.11	1.33	1.31	1.02	0.74
Cullis R§		0.812	0.745	0.758	0.818	0.904

Refinement		*Structure and stereochemistry*	
Resolution (Å)	20.0–2.0	Number of atoms	
Number of		Protein	1,786
reflections		Carbohydrate	28
Working	18,928	Water	191
Free	1,393	Zinc ions	3
$R_{work}/R_{free}\|$ (%)	22.3/26.4	RMSD bond lengths (Å)	0.014
		RMSD bond angles (degrees)	2.90

*$R_{sym} = \Sigma\Sigma_j |I_j - \langle I \rangle| /\Sigma I_j$, where I_j is the intensity measurement for reflection j and $\langle I \rangle$ is the mean intensity for multiply recorded reflections.   †$R_{iso} = \Sigma |F_{ph} - F_p| /\Sigma |F_p|$, where F_{ph} and F_p are the derivative and native structure factors, respectively.   ‡Phasing power = $\langle F_h \rangle /E$, where $\langle F_h \rangle$ is the root-mean-square heavy-atom structure factor and E is the residual lack of closure error.   §Cullis $R = \Sigma ||F_{ph} \pm F_p| - |F_{h,c}|| /\Sigma |F_{ph} \pm F_p|$, where $F_{h,c}$ is the calculated heavy-atom structure factor. $\|R_{work, free} = \Sigma ||F_{obs}| - |F_{calc}|| / |F_{obs}|$, where the working and free R factors are calculated with the working and free reflection sets, respectively. The free reflections (6.9% of the total) were held aside throughout refinement.
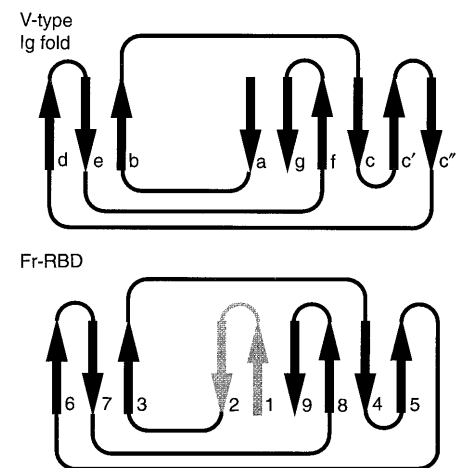

Fig. 3. Topological relation between Fr-RBD and the Ig fold. Side views of the topologies of a v-type Ig fold and of Fr-RBD are shown with the β sandwiches splayed open between strands c″ and d in the Ig fold and between strands 5 and 6 in Fr-RBD. Strand c″ of the v-type Ig fold can be replaced by a loop (*38*), as is the case in Fr-RBD. Strand a of the v-type Ig fold can be associated with either sheet (*38*); only one alternative is shown. Strands 1 and 2 of Fr-RBD are shown in light gray to indicate that they are a modification of the v-type Ig-fold topology (*38*).

Fig. 4. The putative receptor-binding surface. A molecular surface is superimposed on the structure of the region containing likely receptor-contacting residues. Residues Arg[85], Glu[89], Pro[90], and Thr[92] form a ridge across the top of this region. The face just below the ridge contains the critical Asp[86], which lies adjacent to a hydrophobic pocket. This pocket is lined with the residues Pro[90], Leu[94], and Trp[102], as well as Asp[86], and its base is formed by Leu[91]. The relation of the putative receptor-binding surface to the intact domain can be derived from the inset, in which the expanded region is boxed in red, and the helices are lettered as in Figs. 1 and 2A. The orientation is roughly a 180° rotation about the *y* axis from the views in Fig. 2. The figure was generated with Grasp (*39*).

ditions as a cryo-protectant. The solvent content of the crystals was about 52%. The Fr-RBD model contains all residues in the fragment except the first eight at the NH_2-terminus and the COOH-terminal residues from the factor Xa cleavage site. The model contains one N-acetylglucosamine (GlcNAc) at each of the two N-linked glycosylation sites, residues 12 and 168 (*10*). There is clear electron density in the molecular isomorphous replacement (MIR) map for the first GlcNAc at position 168, but density is not visible for additional carbohydrate units. One GlcNAc was placed at position 12, but the precise orientation of this carbohydrate unit should be considered ambiguous because it is difficult to interpret its electron density. Three zinc ions were bound in the Fr-RBD crystals: one at His[55] and two at sites spaced 3.58 Å apart from one another at a crystal contact, bridging Asp[21] and Ser[51] of one molecule and Asp[86] of another. Data to 2.8 Å were subsequently collected on a crystal grown in calcium acetate. The lengths of unit cell edges b and c were decreased in these crystals by 2.8 and 3.9%, respectively (a = 55.3 Å, b = 66.5 Å, c = 77.3 Å, α = β = γ = 90°). Molecular replacement with the program Amore (*25*) and refinement to a free R factor of 29.4% demonstrated that the packing is shifted slightly but significantly in these crystals, diminishing the distance between symmetry-related molecules and eliminating the intersubunit zinc ion-binding sites. Therefore, the zinc ion-binding sites are not integral to the Fr-RBD structure. There are no significant differences between the protein structures refined against data from the zinc- or calcium-containing crystals.

9. Although strand 3 contains two prolines that prohibit it from being considered a β strand according to standard secondary structure classification schemes such as that of Kabsch and Sander (*26*), we consider it a β strand here because it is in a position to make four backbone hydrogen bonds to strand 7.

10. M. Linder, D. Linder, J. Hahnen, H.-H. Schott, S. Stirm, *Eur. J. Biochem.* **203**, 65 (1992). Four disulfide bonds (cysteines 46 and 98, 72 and 87, 73 and 83, and 178 and 184) are in the helical lobe, whereas two disulfide bonds (cysteines 121 to 141 and 133 to 146) are in a loop between strands 4 and 5. Only one cysteine, at position 121, lies in a β strand.

11. L. Holm and C. Sander, *J. Mol. Biol.* **233**, 123 (1993); *Nucleic Acids Res.* **24**, 206 (1996). The 3D-ali server, a network service for comparing protein structures in three dimensions, is available at www.embl-heidelberg.de/argos/ali/al.html.

12. The following proteins gave z scores ranging from 3.4 to 2.0 and α-carbon root mean square deviations (RMSDs) between 3.1 and 4.9 Å over about 90 residues each (an alignment was found for strands 3 through 9, but the helical lobe and strands 1 and 2 could not be aligned): single-chain FV fragment, light chain (pdb1mfa.ent); human CD2 (pdb1hnf.ent); OPG2 Fab fragment, heavy chain (pdb1opg.ent); rat CD4, domain 3 (pdb1cid.ent); human CD8, domain 1 (pdb1cd8.ent); Fab fragment, light chain (pdb1mlb.ent); beta chain of murine T cell antigen receptor, variable domain (pdb1bec.ent); human CD4, domain 1 (pdb3cd4.ent); human coagulation factor XIII (pdb1ggt.ent); *E. coli* PAP*D chaperone (pdb3dpa.ent); human p53 tumor suppressor protein (pdb1tup.ent); human VCAM-1, domain 1 (pdb1vca.ent); and murine N-cadherin, domain 1 (pdb1nci.ent).

13. These variable regions have previously been referred to as VRA and VRB (*27*). Biased by the Fr-RBD structure and given the existence of a conserved region near the end of VRA, we divided VRA into two distinct variable regions, one that we still refer to as VRA and the other that we now call VRC.

14. D. Ott and A. Rein, *J. Virol.* **66**, 4632 (1992).

15. C. Peredo, L. O'Reilly, K. Gray, M. J. Roth, *ibid.* **70**, 3142 (1996); R. A. Morgan *et al.*, *ibid.* **67**, 4712 (1993).

16. We generated a packing model for Fr-RBD as it would exist in the trimeric envelope glycoprotein complex. We constructed this trimer packing model manually by placing the carbohydrates (*10*) toward solvent, keeping variable sequences surface-exposed rather than at trimer contacts and maximizing

new receptor specificities and tropisms has already been demonstrated by the success of viral evolution in generating the receptor diversity of this subgenus.

REFERENCES AND NOTES

1. E. Hunter and R. Swanstrom, *Curr. Top. Microbiol. Immunol.* **157**, 187 (1990).

2. A. E. Smith, *Annu. Rev. Microbiol.* **49**, 807 (1995).

3. MLVs have been grouped on the basis of superinfectivity resistance, the phenomenon whereby cells preinfected with an MLV cannot be infected by an exogenous virus that presumably utilizes the same receptor. These groups have been named according to their host ranges: ecotropic, amphotropic, polytropic, and xenotropic. Fr-MLV is an ecotropic MLV and infects only murine and certain other rodent cells. Amphotropic and polytropic viruses infect both murine and nonmurine cells, whereas xenotropic viruses infect only nonmurine cells.

4. L. M. Albritton, L. Tseng, D. Scadden, J. M. Cunningham, *Cell* **57**, 659 (1989); J. W. Kim, E. I. Closs, L. M. Albritton, J. M. Cunningham, *Nature* **352**, 725 (1991); H. Wang, M. P. Kavanaugh, R. A. North, D. Kabat, *ibid*., p. 729.

5. The NH_2-terminal domain of SU expressed in isolation is sufficient to mediate superinfectivity resistance in both ecotropic and amphotropic MLVs (*21*). Furthermore, this domain binds MCAT-1 in vitro (*6*).

6. R. A. Davey, C. A. Hamson, J. M. Cunningham, *J. Virol.*, in press.

7. A. Pinter, W. J. Honnen, J.-S. Tung, P. V. O'Donnell, U. Hammerling, *Virology* **116**, 499 (1982).

8. We expressed in insect cells, from a baculovirus vector, a truncated form of the ecotropic envelope from the Friend isolate (GenBank accession number

J02192) (*22*). The coding sequence was fused in-frame to a factor Xa protease site (IEGR), three copies of the hemagglutinin epitope (YPYDVPYA) (*23, 24*), and a six-histidine motif. Details of this vector and of protein production will be provided elsewhere (*6*). Briefly, insect cells in logarithmic growth phase were infected with the recombinant virus. Culture supernatants were collected 3 days after infection, protein was purified over a nickel-primed chelating resin (Pharmacia), and the tags were removed with factor Xa protease (New England Biolabs, Beverly, MA). Cleaved protein, containing residues 1 through 236 of mature Fr-MLV, as well as six additional residues remaining on the COOH-terminus from the factor Xa cleavage site, was repurified by means of a Mono S ion exchange column (Pharmacia). The eluted protein was dialyzed against 20 mM sodium acetate (pH 5.5) and concentrated to 10 mg/ml with a centricon-3 microconcentrator (Amicon, Beverly, MA). We initially grew crystals of Fr-RBD by the hanging drop method at 20°C by equilibrating over a reservoir containing 150 mM calcium acetate, 100 mM sodium cacodylate (pH 6.5), and 19% polyethylene glycol 8000. In 3 to 4 days, crystals with a long rodlike or needlelike morphology appeared. When zinc acetate was substituted for calcium acetate in the well solution, crystals did not grow readily, and the crystals that were observed were clustered. However, streak-seeding with a human eyelash from the crystals grown in the presence of calcium to protein that had been preequilibrated for 12 hours in zinc solution yielded single blocklike crystals in the space group $P2_12_12_1$ (a = 55.3 Å, b = 68.4 Å, c = 80.4 Å, α = β = γ = 90°), with a single Fr-RBD monomer in the asymmetric unit. Subsequent crystals were grown by streak-seeding either from crystals grown in calcium or from zinc crystals that were themselves grown by streak-seeding. Seven percent glycerol was later included in the crystallization con-

the contact area while avoiding steric clashes. Although VRC is distant from VRA and VRB within an Fr-RBD monomer, VRC from one subunit is close to VRB of the adjacent subunit of the trimer model, such that there are only three variable lobes per trimer, with each being composed of sequences from two Fr-RBD subunits (D. Fass, thesis, Massachusetts Institute of Technology, Cambridge, 1997).

17. A. J. MacKrell, N. W. Soong, C. M. Curtis, W. F. Anderson, *J. Virol.* **70**, 1768 (1996).
18. MacKrell and co-workers (*17*) have also identified two mutants, His[123] and Arg[124] (His[125] and Arg[126] in Fr-MLV SU), that severely reduce incorporation of envelope glycoproteins into virions, consistent with the mutant glycoproteins having defects in folding or assembly. The side chain of His[125] in Fr-RBD is located near a buried aspartic acid, Asp[161], that is conserved among all MLVs. Replacing His[125] with a different hydrophobic residue would isolate the buried charge of Asp[161], potentially destabilizing VRC, the core of the domain, or both regions. The other structurally significant residue, Arg[126], is partially buried and in position to form a hydrogen bond to the backbone carbonyl of residue 134. This interaction could anchor the VRC loop or aid in proper disulfide bond formation of nearby cysteines and is apparently also critical for proper folding and processing.
19. S. Valsesia-Whittman *et al.*, *J. Virol.* **70**, 2059 (1996).
20. N. Kasahara, A. M. Dozy, Y. W. Kan, *Science* **266**, 1373 (1994).
21. J. M. Heard and O. Danos, *J. Virol.* **65**, 4026 (1991); J.-L. Battini, O. Danos, J. M. Heard, *ibid.* **69**, 713 (1995).
22. C. Friend, *J. Exp. Med.* **105**, 307 (1957); W. Koch, G. Hunsmann, R. Friedrich, *J. Virol.* **45**, 1 (1983).
23. Single-letter abbreviations for the amino acid residues are as follows: A, Ala; D, Asp; E, Glu; G, Gly; I, Ile; P, Pro; R, Arg; V, Val; and Y, Tyr.
24. D. J. Goldstein and R. Schlegel, *EMBO J.* **9**, 137 (1990).
25. J. Navaza, *Acta Crystallogr. Sect. A Found. Crystallogr.* **50**, 157 (1994).
26. W. Kabsch and C. Sander, *Biopolymers* **22**, 2577 (1983).
27. J.-L. Battini, J. M. Heard, O. Danos, *J. Virol.* **66**, 1468 (1992).
28. Z. Otwinowski, in *Data Collection and Processing*, L. Sawyer, N. Isaacs, S. Bailey, Eds. [Science and Engineering Research Council (SERC), Daresbury Laboratory, Warrington, UK, 1993], pp. 56–62.
29. Collaborative Computational Project, Number 4, *Acta Crystallogr. Sect. D Biol. Crystallogr.* **50**, 760 (1994).
30. Z. Otwinowski, in *Isomorphous Replacement and Anomalous Scattering*, W. Wolf, P. R. Evans, A. G. W. Leslie, Eds. (SERC Daresbury Laboratory, Warrington, UK, 1991), pp. 80–86.
31. K. Cowtan, *Joint CCP4 ESF-EACBM Newsl. Protein Crystallogr.* **31**, 34 (1994).
32. T. A. Jones and M. Kjeldgaard, *O—The Manual* [online], Uppsala, Sweden, 1992. Available at www.imsb.au.dk/~mok/o.
33. A. T. Brünger, *X-PLOR Version 3.1. A System for X-ray Crystallography and NMR* (Yale Univ. Press, New Haven, CT, 1992).
34. 3/M, *Nature* **355**, 472 (1992).
35. K. Y. Zhang and D. Eisenberg, *Protein Sci.* **3**, 687 (1994).
36. M. Carson, *J. Appl. Crystallogr.* **24**, 958 (1991).
37. P. Kraulis, *ibid.*, p. 924.
38. P. Bork, L. Holm, C. Sander, *J. Mol. Biol.* **242**, 309 (1994).
39. A. Nicholls, K. A. Sharp, B. Honig, *Proteins* **11**, 281, 1991.
40. We thank S. C. Harrison, S. J. Gamblin, and D. C. Wiley for helpful discussions and N. Azubuine for media preparation. J.M.B. is a Whitehead Fellow and acknowledges support from the W. M. Keck Foundation. This work was funded by the Howard Hughes Medical Institute and utilized the W. M. Keck Foundation X-ray Crystallography Facility at the Whitehead Institute. The coordinates have been deposited in the Protein Data Bank with accession number 1AOL.

16 April 1997; accepted 12 July 1997

The Importance of Recent Ice Ages in Speciation: A Failed Paradigm

John Klicka and Robert M. Zink

Late Pleistocene glaciations have been ascribed a dominant role in sculpting present-day diversity and distributions of North American vertebrates. Molecular comparisons of recently diverged sister species now permit a test of this assertion. The Late Pleistocene Origins model predicts a mitochondrial DNA divergence value of less than 0.5 percent for avian sister species of Late Pleistocene origin. Instead, the average mitochondrial DNA sequence divergence for 35 such songbird species pairs is 5.1 percent, which exceeds the predicted value by a factor of 10. Molecular data suggest a relatively protracted history of speciation events among North American songbirds over the past 5 million years.

Evidence from molecular systematics has provided fresh insights into several long-standing controversies regarding avian evolution, including the origin of birds (*1*), the origin and distribution of modern-day avian orders (*2*), and the survival of avian lineages across the Cretaceous-Tertiary boundary (*3*). The timing of the origin of modern bird species remains unclear. Many authors (*4*, *5*) postulate a recent origin for North American songbird species (Order Passeriformes) and species complexes.

These origins are typically associated with Late Pleistocene glacial cycles (*6–8*) involving (i) fragmentation of a widespread ancestral species into refugia during periods of glacial advance and (ii) subsequent genetic divergence among small isolated populations, followed by (iii) range expansion during interglacials. Typically, one [beginning circa (ca.) 100,000 years ago] or two (ca. 250,000 years ago) such cycles are invoked. This model, here termed the Late Pleistocene Origins (LPO) model, is widely accepted today [see (*9*) for example].

If mitochondrial DNA (mtDNA) evolves at a clocklike (*10*) rate of 2% per million years (My) (*11*), then a plot of divergence values for sister species of Late Pleistocene origin should be strongly left-skewed and leptokurtic. Invoking either one or two glacial cycles, mtDNA sequences of species pairs should differ on average by 0.2 to 0.5%. The LPO model also predicts that phylogenetic analyses of mtDNA sequences (haplotypes) from recently separated species will result in trees that do not reflect recognized species (taxonomic) limits. That is, haplotypes in one species can be more closely related to haplotypes in the sister species than to those in their own (*12*). We tested the LPO paradigm directly by analyzing most of the

J. F. Bell Museum of Natural History and Department of Ecology, Evolution, and Behavior, University of Minnesota, 1987 Upper Buford Circle, St. Paul, MN 55108–6097, USA.

songbird taxa used to construct it. Table 1 depicts all North American songbird species (*13*) for which Late Pleistocene origins have been postulated (*4*, *5*) and for which comparative mtDNA data (*14*) are now available (*16–19*). These comparisons represent the best estimates of divergence times among what are presumed to be the most recently evolved songbird species. The plot of observed divergence values (Fig. 1) is neither left-skewed nor leptokurtic. The average percent divergence for the 35 taxon pairs is 5.1% (SD ± 3.0), which suggests an average Late Pliocene divergence time of 2.45 million years ago (Ma) (*20*). This estimated divergence time and a divergence time consistent with a Late Pleistocene origin differ by an order of magnitude. Alternatively, if the molecular clock is improperly calibrated and our average percent divergence does correctly reflect genetic change occurring since the beginning of the last glacial advance (assume 5.1% change per ca. 100,000 years), two taxa isolated for 1 My would differ by 50%. Multiple substitutions at the same nucleotide position and eventual DNA saturation make a figure this high improbable, and no such saturation effects were detected in the taxon pairs examined.

An additional test of the LPO model derives from comparing the 35 "Late Pleistocene" species pairs with 13 pairs of species not specifically theorized to have evolved in the Late Pleistocene (*21*). The mean mtDNA pairwise distance for these presumably older songbird pairs is 5.2% (SD ± 2.3), a value not significantly different from that of the 35 "Late Pleistocene" pairs (Mann-Whitney U test, $P = 0.48$). Furthermore, the distributions of mtDNA distances for the two groups are not different (Kolmogorov-Smirnov two-group test; $\chi^2 = 1.4$, df = 2, $P = 0.50$). These results contradict the expectations of the LPO model. Overall, these data